The Behavior of Ni, Ni-60Co, and Ni_3Al during One-Dimensional Shock Loading

J.C.F. MILLETT, N.K. BOURNE, and G.T. GRAY III

The response of pure nickel (Ni), a binary Ni-60 at. pct cobalt (Co) alloy exhibiting a low stacking fault energy (SFE), and the ordered face-centered-cubic (fcc) alloy Ni-24Al-0.01B to shock loading has been studied using the technique of plate impact. Changes in the variation of mechanical properties with shock amplitude and pulse duration have been explained in terms of a shift from dislocation dominated to twin dominated plasticity in the case of the Ni-Co alloy and the increasing effect of brittle failure in the case of Ni_3Al.

DOI: 10.1007/s11661-007-9427-8

I. INTRODUCTION

THE response of materials to high loading rate situations has been a source of much interest since World War II. Typically, this has concentrated in the fields of ballistics and armor development, but more recently applications such as crash test worthiness, high rate forming and machining, satellite protection, and the aerospace industry have also made investigations in this area. In particular, the development of jet turbine engines requires knowledge of the response of materials to impact events of importance to understanding and developing predictive models describing material response under bird strike, foreign object damage, and blade containment loading environments.

Shock wave testing of materials can be performed using a variety of techniques including explosive loading, and more commonly using launcher-driven plate impact. This technique uses a flat and parallel flyer plate, which is accelerated down a smooth bore gun either by a powder propellant breech or by using compressed gas. It is impacted onto an equally flat and parallel target plate, which is aligned to the flyer to a tolerance of less than 1 mradian (25 μm over 50 mm or 5 optical fringes). At high impact velocities (100 m s^{-1} and greater) a planar shock wave is generated, behind which conditions of one-dimensional (1-D) strain prevail (assuming the material is isotropic) until release waves from the edge of the target reach the measurement location. Under these conditions, the strain (ε) is accommodated down the impact axis while the strains perpendicular to it are zero due to inertial confinement. As a consequence, there must be a confining stress (σ) operating in these directions; thus,

$$\varepsilon_x \neq 0 = \varepsilon_y = \varepsilon_z \text{ and } \sigma_x \neq \sigma_y = \sigma_z \neq 0 \qquad [1]$$

where x refers to the loading axis and y and z refer to the orthogonal directions to x. A more complete description of materials under shock loading conditions can be found in the review article of Davison and Graham.[1]

The response of any material to external loading, at quasi-static strain rates or the extreme conditions of shock loading, will be governed by the microstructural features it possesses, such as crystalline structure, grain size, second phases, or previous strain history (*i.e.*, dislocation and or twin density). The properties of metallic materials are often manipulated by the addition of alloy elements, and thus the effects of solution strengthening and precipitation hardening have been studied for a great many years. While such research has been performed in great detail for materials designed for applications under more conventional loading regimes, similar work for high-strain rate and impact/shock-loading applications (*i.e.*, armor and armor defeat from the military, bird strike and blade containment in the aerospace industry, and satellite protection from orbital debris) is developed to a much lesser degree. For this reason we have chosen to investigate the response of nickel (Ni) and two of its alloys to shock loading.

As a pure face-centred-cubic (fcc) metal, Ni has received in-depth study, and its behavior under shock loading (discussed in more detail subsequently), both mechanically and microstructurally is reasonably well understood. The two alloys we investigate are Ni-60 at. pct cobalt (Co), and Ni-24 at. pct aluminum-0.01 at. pct boron. In the case of the first alloy, Co was chosen as an addition for the following reasons. Although Co itself possesses a hexagonal-close-packed (hcp) structure, at 60 at. pct Co the alloy itself is fcc from room temperature to its melting point.[2] In addition, Ni and Co atoms are similar in terms of atomic number (28 and 27, respectively), atomic weight (58.69 and 58.93 ram), and atomic radii (135 pm for both). As this is a substitutional alloy, Co additions to Ni lead to small local atomic mismatches. However, data presented by Gallagher[3] show that Co alloying additions reduce the stacking fault energy (SFE, γ) in Ni significantly from ~200 ergs cm^{-2} to between 20 to 80 ergs cm^{-2} at 60 at. pct Co. The SFE is known to have a major influence on

J.C.F. MILLETT, Senior Scientist, and N.K. BOURNE, Distinguished Scientist, are with the AWE, Aldermaston, Reading RG7 4PR, United Kingdom. G.T. GRAY III, Laboratory Fellow, is with the MST-8, Los Alamos National Laboratory, Los Alamos, NM 87545, USA. Contact e-mail: Jeremy.Millett@awe.co.uk
Manuscript submitted September 8, 2007.
Article published online December 28, 2007

the mobility and cross-slip propensity of dislocations, through the spacing of partial dislocations, d:

$$d = \frac{\mu a^2}{24\pi\gamma} \quad [2]$$

where μ is the shear modulus and a is the lattice parameter. As partial dislocations must travel as pairs, wider spacing increases the difficulty of their motion and the likelihood of tangling due to a reduced ease of cross-slip. Therefore, at quasi-static strain rates, this results in increased work-hardening rates. Under shock loading conditions, the most thorough work investigating the role of SFE was performed on copper-aluminum alloys by Rohatgi and his colleagues.[4–7] As aluminum content increased to 6 wt pct, SFE reduced from 78 ergs cm^{-2} in pure copper to 6 ergs cm^{-2}. At shock stresses of 10 and 30 GPa, it was found that these alloys showed an increased propensity to twin as aluminum content increased and thus SFE decreased, with only alloys of less than 0.2 wt pct aluminum deforming purely by dislocation generation and storage. Recovered samples deformed purely in 1-D strain[4,6] were mechanically tested and compared to the annealed reference state, taking into account the imposed shock strain. It was observed that in these recovered samples, the increased strength (due to shock loading) decreased but the work hardening increased as the SFE decreased. In the high SFE alloys and pure copper, it was suggested that the rapid increase in dislocation density during the shock saturated the substructure and thereafter reduced the ability for the material to generate and store new dislocations when reloaded. In the low SFE materials, much of the shock deformation was accommodated by deformation twinning. Thus, when reloaded at quasi-static strain rates deformation could be accomplished by further dislocation generation. This was further confirmed by differential scanning calorimetry (DSC).[4]

Although the existing literature on the shock response of Ni-Co alloys is not extensive, the best example being that of Trunin *et al.*,[8] Ni itself has been studied extensively. The effect of prior cold rolling on the shock loading of Ni was studied by Rose *et al.*[9] The hardness of recovered samples of shocked samples was observed to reach a near constant level, *i.e.*, the saturation stress, regardless of the prior degree of cold work. This led them to suggest that stacking faults and twins did not contribute significantly to the shock-hardening process. However, Kressel and Brown[10] demonstrated that the dislocation and point defect concentration increased approximately eightfold in shock-loaded Ni, when compared to that of a cold-rolled equivalent at 0 °C, taking into account the equivalent plastic strain. Grace[11] also showed that shock-loaded Ni (and indeed copper) experienced pronounced hardening compared to the unshocked material.

More significantly, Murr and Kuhlmann-Wilsdorf[12] examined the shocked microstructure of Ni as a function of pulse amplitude and duration. Deformation was observed to occur *via* dislocation generation and storage, with the dislocations arranging themselves upon relaxation into cell walls. At 25 GPa, dislocation density and cell size was seen to be near constant with increasing pulse duration. However, below durations of ~0.5 μs, the deformation structure was not fully developed, which suggests that there was a time dependence in the shock response. This reasoning is consistent with the research of Wright and Mikkola[13] on Cu-Ge alloys shocked for short pulse durations. The authors suggest that steady-state conditions were achieved at ~1 μs. Dislocation cell size was also observed to be inversely proportional to shock amplitude. Greulich and Murr[14] further showed that the initial microstructure (in terms of grain size or orientation) had little effect upon the final shocked microstructure. Twins were also noted at stresses above 35 GPa, forming in grains that were preferentially orientated such that the [001] crystallographic zone axis was parallel to the loading axis. Twin formation itself increased with peak shock stress amplitude and grain size. Below this stress, the residual (post shock) yield strength displayed a Hall–Petch-type relationship with original grain size. Where twinning occurred, the intertwin spacing was also seen to follow a Hall–Petch-type relationship with the postshock yield strength, in agreement with the more recent work of Rohatgi and his colleagues.[4–7]

The effects of temperature on the shock response of Ni have been investigated by Meyers *et al.*[15] at temperatures of 77 and 300 K. At 77 K, cells were seen to be less well developed. Their results also indicated that cell size was dependent upon pulse duration, although they conceded that this may be due to deviations from 1-D strain caused by inadequate lateral momentum trapping. Follensbee and Gray[16] used carefully controlled momentum trapping techniques[17] while quantifying the shock hardening behavior of Ni with two grain sizes (40 and 225 μm) and two single-crystal orientations to the loading axis ($\langle 111 \rangle$and $\langle 100 \rangle$). As was shown by the previous investigations, defect generation and storage in these Ni-based materials was seen to occur *via* dislocation generation and dislocation cell formation, respectively. When compared on a resolved shear stress-shear strain basis, little difference in the magnitude of shock hardening was seen due to grain size or crystallographic orientation in the case of the two single crystals, although cell size was noted to be somewhat smaller in the single crystals. Compared to pure Ni, alloys such as Ni-20 pct Cr and Ni-16 pct Cr-7 pct Fe, were shown to display a greater propensity of deformation twinning,[18] consistent with the reduction of SFE, as discussed previously concerning copper-aluminum alloys.[4–7]

The shock response of complex ordered Ni-based alloys, such as superalloys (*i.e.*, Mar-M200), has been investigated only in terms of their shock response such as the Hugoniot elastic limit (HEL, the yield strength under 1-D strain) and spall (shock-induced tensile) strength. Dandekar and Martin[19] showed that the HEL of Mar-M200 underwent significant precursor decay (*i.e.*, reducing with specimen thickness). Zaretsky *et al.*[20] examined the mechanical behavior of two superalloys as a function of temperature. They showed that the strength of these materials gradually decreased with temperature until reaching an abrupt reduction between 550 °C and 600 °C. This was ascribed to

variations in the heat capacity associated with the equilibration of short-range order in the fcc matrix of these materials. These data raise questions concerning the behavior of the hardening phase in superalloys, the ordered fcc intermetallic compound based on the composition Ni_3Al.

A wealth of literature has investigated the mechanical and microstructual response of Ni_3Al to mechanical loading at quasi-static strain rates,[21–23] including its well known positive dependence of strength upon temperature explained by the Kear–Wilsdorf locking mechanism,[24] whereby $a/2[110]$ dislocations on the {111} planes cross-slip onto the {100} planes where they are effectively sessile. As cross-slip is thermally activated, this mechanism explains how strength increases with temperature. Also, Ni_3Al has been shown to be capable of achieving useful levels of ductility through careful alloying by Aoki *et al.*,[21] through a slight reduction in the aluminum content and small additions of boron (~0.1 wt pct). Research to date on the high strain rate response of Ni_3Al and its derivatives is more scarce. Sizek and Gray[25] examined its behavior under quasi-static and intermediate strain rates (0.01 to 8000 s^{-1}) using the split Hopkinson pressure bar (SHPB). They demonstrated that the positive temperature dependence of strength occurred over the entire strain rate range. However, at higher strain rates, the flow stresses did not reach a peak at ~600 °C, but rather continued to climb. They suggested that this is due to the suppression of dynamic recovery processes at these high strain rates. At low (room temperature and below) temperatures, yield strength was seen to vary only slightly with strain rate. This was attributed to the low Pierel's stress on the dominant ⟨110⟩{111} slip system, further confirmed by microstructural analysis. At higher strain rates, strength was observed to be more strain rate dependent, presumably as the ⟨110⟩{100} slip system became more influential.

Under shock loading conditions, Gray[26] shock prestrained and recovered Ni_3Al samples under conditions of 1-D strain. As with pure Ni, he showed that it displayed enhanced hardening compared to the undeformed material. In a later work, Albert and Gray[27] used transmission electron microscopy (TEM) to show that under shock loading the preferred deformation mode was planar slip on the {111} planes. In addition, deformation was accommodated by twin formation, also on the {111} planes with an assumed direction of ⟨112⟩. Katsantseva *et al.*[28] shocked and recovered single crystals of a superalloy, consisting of approximately 90 pct by volume of Ni_3Al. By loading up to a maximum of 100 GPa, they indicated that there was a phase transition from the fcc $L1_2$ structure to the tetragonal $D0_{22}$ phase. Computational work by Geng *et al.*[29] also suggested that there is an order-disorder reaction at ~205 GPa. Finally, a body of work has considered shock-induced chemical formation of Ni_3Al from elemental powders.[30,31]

In a series of articles, the authors have investigated the effect of shock loading on Ni and its alloys with Co[32,33] and aluminum.[34] The purpose of this article is to discuss the influence of alloying and crystallographic order on the shock response of Ni, Ni-60Co, and Ni-24Al-0.01B.

II. EXPERIMENTAL TECHNIQUES

All shock loading experiments were performed by launching flyer plates of either dural (aluminum alloy 6082-T6) or copper (flat and parallel to ± 5 μm) into equally accurately machined plates of the target materials. Dural and copper were chosen as flyer materials because their shock responses are well documented in the literature.[35] The impactors were attached to polyoxymethylene sabots with a recessed front surface to ensure that the rear of the flyers was unconfined. These were launched at velocities of 180 to 900 m s^{-1}, using a single stage, 50-mm bore, 5-m long gas gun.[36]

A. *Equation-of-State Measurements*

Experiments were performed to determine the variation of impact stress (σ_x) and shock velocity (U_S) with particle velocity (u_p, the velocity of material flow behind the shock front) for the three materials studied. A manganin stress gage (MicroMeasurments type LM-SS-125CH-048, Measurements Group UK, Ltd., Basingstoke, United Kingdom) was either placed between ~5-mm plates of the target material or supported on the rear of the target plate with a 12 plate of polymethylmethacrylate (PMMA), with the gage offset into the PMMA by ~1.5 mm to act as further protection. A second gage was supported on the front of the target with a 1-mm-thick plate of either dural or copper, matched to the material of the flyer. In this way, that gage would experience the internal stress within the target itself. The shock velocity was determined from the known thickness of the sample (Δw) and the temporal spacing of the traces (Δt), taking into account the degree of insulation around the gages ($U_S = \Delta w/\Delta t$). Gage calibrations were according to the work of Rosenberg *et al.*[37] The Hugoniot (variation of stress with particle velocity) was determined using impedance matching techniques, assuming conservation of momentum across the flyer/target interface.

B. *Spallation Measurements*

Flyer and target geometries were chosen such that the release fans from the rear of the flyer and target met in the middle of the target plates. Variations of pulse duration were achieved by varying the thickness of the flyer/target pairs, and stress amplitude by employing different flyer plate velocities. Measurements were made by supporting manganin stress gages (MicroMeasurments type LM-SS-125CH048) on the rear of the target plates with 12 mm of PMMA, with the gage backed into the PMMA by ~1.5 mm. Gage calibrations were as discussed previously. As the gage measurements were made in the PMMA, they were converted to in-material values using the dynamic impedances ($Z = \rho U_S$) of the PMMA and the target material, and the measured stress values (σ_P); thus,

$$\sigma_{\text{material}} = \frac{Z_P + Z_m}{2Z_P}\sigma_P \quad [3]$$

where m refers to the state within the material itself.

C. *Lateral Stress and Shear Strength Measurements*

The 8-mm plates of the target materials were sectioned in half, and a manganin stress gage (MicroMeasurments type J2M-SS-580SF-025) was introduced ~4 mm from the impact face. Targets were then reassembled using a low viscosity epoxy adhesive and held in a special jig for a minimum of 12 hours. The impact faces were then lapped such that they were flat to a maximum of 5 fringes from a monochromatic light source. In this orientation, the gages were sensitive to the lateral (or confining) component of stress (σ_y). From prior knowledge of the Hugoniot, the shear strength (τ) can be determined through the well-known relation:

$$2\tau = \sigma_x - \sigma_y \quad [4]$$

Voltage-time data from the gages were converted to stress-time using the methods of Rosenberg and Partom,[38] with a modified analysis that does not require prior knowledge of the impact conditions.[39] In addition, in a very recent work,[40] we have shown that the geometry of the stress gage at low stresses can influence the final result and consequently must be accounted for. Finally, the experimental error on the gage traces has been quoted at ~2 pct.[37] Additional errors will occur through inaccuracies in thickness measurements, precise thickness of the gage layer (a combination of the gage element itself, the insulating layers around it and the precise thickness of the epoxy adhesive), and small misalignments between the flyer plate and target assembly. These will have a cumulative effect, but we believe that the maximum error on the gage records is ~5 pct.

Further details of all three experimental sets can be found in previous publications.[32–34] A schematic diagram of the target assemblies is presented in Figure 1. All materials were characterized before shock loading in terms of their sound speeds, using quartz transducers operating at 5 MHz, employing a Panametrics PR5077 pulse receiver (Panametrics, Coventry, United Kingdom). Some of the samples were recovered afterwards for subsequent metallographic analysis. It should be emphasised that the full 1-D recovery techniques developed by Gray[41] were not used. However, it was felt that differences noted between these similar materials would still provide valuable initial insight into their different responses to shock loading.

III. MATERIALS DATA

The pure Ni and the Ni-60Co were received in the form of ~60-mm forged bar stock (Special Metals, Wiggins, Hereford, United Kingdom). The original ingots were cast into tapered iron molds and air-cooled. The cast microstructure was broken down by hammer forging at 1080 °C. The Ni_3Al was manufactured from a gas atomised powder, canned in a mild steel container and extruded at 1273 K. Further details concerning the processing of the Ni_3Al can be found in an earlier reference.[25] We present the as-received microstructures for all three materials in Figure 2.

The compositions of the Ni and Ni-60Co are presented in Table I. The composition of the Ni_3Al (in at. pct) was 24.1 pct aluminum, 0.095 pct boron, balance Ni. The acoustic properties are presented in Table II.

It can be seen that the grain sizes in the otherwise similar Ni and Ni-60Co are very different, with that of the alloy being smaller. This can be explained through examination of Eq. [2]. During hot working to break down the cast microstructure, the greater spacing of the partial dislocations in the alloy will restrict their mobility, and hence lead to a greater build up in dislocation density. This, in turn, will increase the propensity for dynamic recrystallization during forging, resulting in a finer forged grain size.

IV. RESULTS

In Figure 3, typical gage traces from an experiment to determine the equation of state, in this case for Ni, impacted with a 5-mm copper flyer plate at 730 ms^{-1} is shown. Both traces can be seen to reach an amplitude of ~15 GPa. The rise time of both gages is approximately 200 ns. This amplitude, along with the time spacing (Δt) was used to determine the equation of state of the three alloys, in terms of shock stress, shock velocity, and particle velocity. In Figure 4, we present the variation of shock velocity with particle velocity for the three materials and also include the Ni data from Marsh[35] for comparison. All three materials over the experimental range studied are seen to display linear U_S-u_p behavior as defined by

$$U_S = c_0 + Su_p \quad [5]$$

where c_0 and S are the shock parameters. It can be seen that the current shock results for the pure Ni are essentially identical to those of Marsh,[35] providing additional confidence in our own measurements. It can also be seen that the response for both Ni and the simple Ni-Co alloy are similar. This is not unexpected as it has been seen in simple binary alloy systems that the equation of state is often similar.[42,43] It is noted that the slope of U_S-u_p for Ni_3Al is somewhat higher than that of Ni and the Ni-60Co alloy, suggesting that this ordered intermetallic material is more compressible. The Hugoniots of the three alloys (also including the data of Marsh for Ni) are presented in Figure 5.

The curve fits are calculated hydrodynamic pressure (P_{HD}), calculated according to

$$P_{HD} = \rho_0 U_S u_p \quad [6]$$

The Hugoniots of these materials are observed to be similar in terms of stress, but the calculated hydrodynamic pressures are more significant. As seen in Figure 5, the behavior of pure Ni and Ni-60Co are

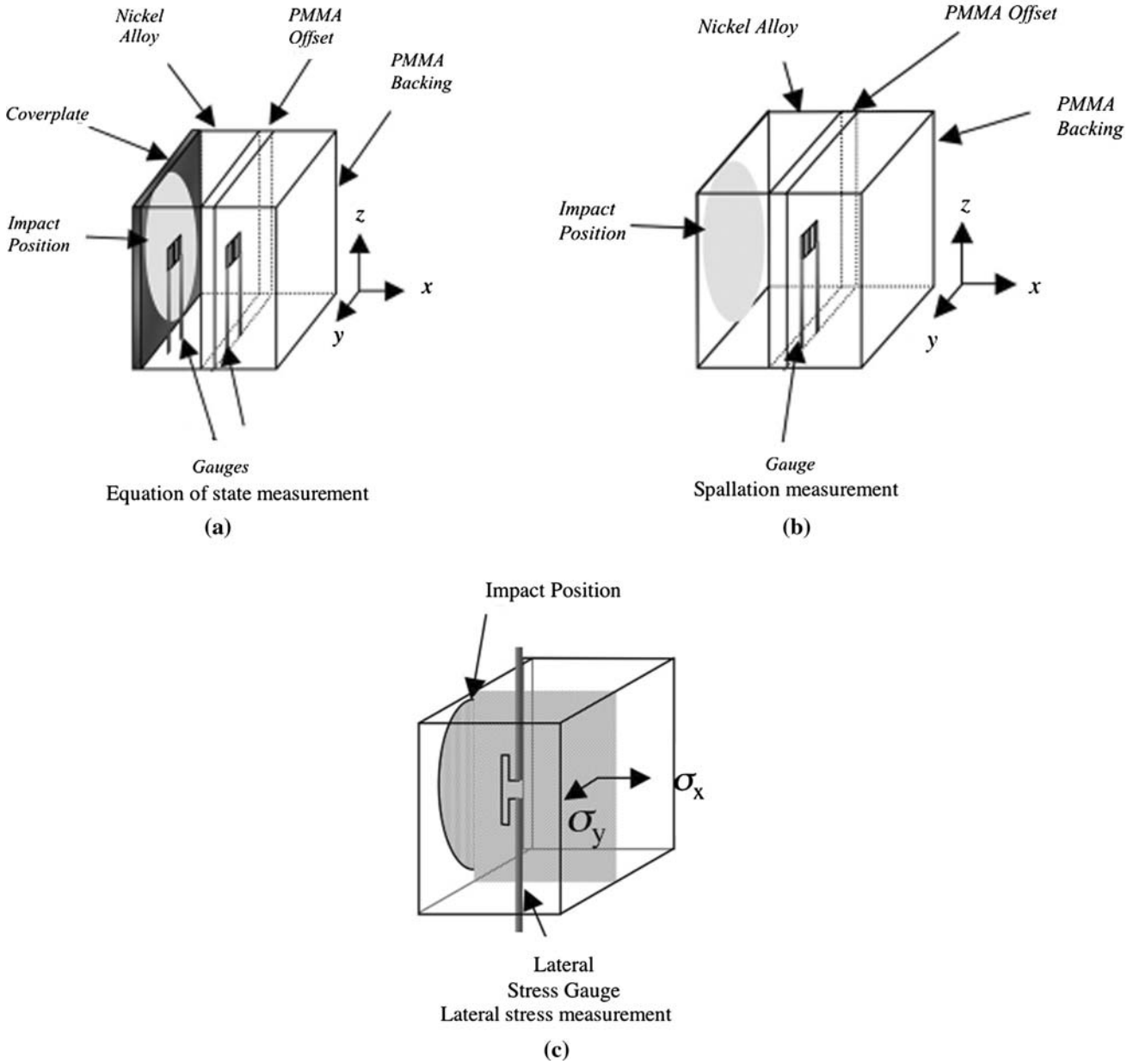

Fig. 1—Schematic of shock targets and gage placements: (*a*) equation-of-state measurement, (*b*) spallation measurement, and (*c*) lateral stress measurement.

essentially indistinguishable, while the slope of the Hugoniot of Ni_3Al is lower, as would be expected from its lower density (Table II) and the higher value of *S*.

In Figure 6, we show representative back surface gage traces from Ni_3Al and Ni-60Co. All three traces display the characteristic "pull-back" signal response in stress that typically characterizes dynamic tensile (spall) failure in shock-loaded materials. In the case of the Ni_3Al traces, a step is also observed on the initial rising part of the traces. This is due to the separation between the elastic and inelastic parts of the shock front, and thus is the elastic limit of the material. Also observe that the level of the elastic limit decreases with shock propagation distance, the so-called elastic precursor decay. No such response is noted in the Ni-60Co trace (or indeed in the pure Ni traces either). We believe that the HEL in both Ni and the Ni-60Co alloy are so low that the stress gages used in this investigation could not resolve them. Also note that in the case of the Ni-60Co trace, there is a sharp dip immediately prior to the rising part of the shock front. This is the result of capacitive linking between the metallic sample and the electrically active stress gage. It is an indication of a rapidly accelerating sample toward the gage, showing the planar nature of the shock front to the gage. A more detailed explanation can be found elsewhere.[44] Figure 7 presents representative lateral stress measurements for all three materials.

The value of stress in the trace label is the impact stress at which the sample was loaded. The three traces presented are typical of the lateral stress responses in all

Pure nickel
(a)

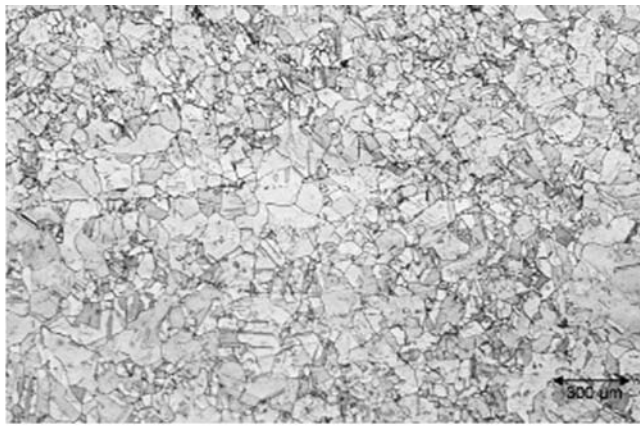

Nickel - 60% cobalt
(b)

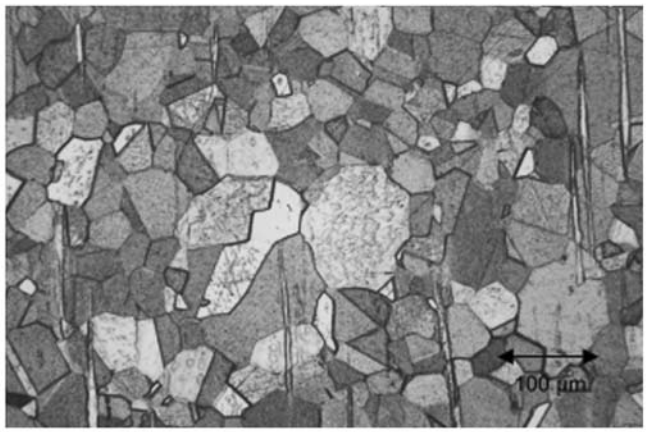

Ni_3Al
(c)

Fig. 2—As-received microstructures of the Ni alloys under investigation: (*a*) pure Ni, (*b*) Ni-60 pct Co, and (*c*) Ni_3Al.

Table I. Composition of Ni and Ni-60Co, in Weight Percent

Pure Ni							
C	Si	Mn	P	S	Al	Co	Cr
< 0.0005	0.002	< 0.001	< 0.001	< 0.001	< 0.001	0.021	< 0.001
Cu	Fe	Mg	Ni	Ti	Pb ppm	Zn ppm	O
0.021	0.008	< 0.001	bal.	< 0.001	< 5	< 10	0.0058
Ni 60 Wt Pct Co							
C	Si	Mn	P	S	Al	Co	Cr
0.004	0.002	< 0.001	< 0.005	< 0.001	< 0.001	bal.	0.001
Cu	Fe	Mo	Nb	Ni	Ta	Ti	V
0.003	0.006	< 0.001	< 0.001	41.9	0.003	< 0.001	< 0.001

three alloys. It can be observed that they all display features in common including a rapid rise to a sharp peak followed by a shallower relaxation in lateral stress behind the shock front before releases enter the gage location and reduce the measured stress back toward ambient. The peak is an electrical effect due to the rapidly rising nature of the shock wave.[44] The relaxation that follows implies an increase in shear strength behind the shock front, according to Eq. [4] and assuming a constant level of longitudinal stress for the pulse duration. Such behavior has been observed in other materials including some intermetallics, such as those based on γ-titanium aluminides[45] and the shape memory alloy NiTi,[46] the engineering alloy Ti-6Al-4V,[47] and some polymers.[48–50] This is an indication that events do not occur instantaneously in the shock front, but rather have a time dependence.

In the subsequent figures, we show how the shock-induced mechanical responses of these three alloys vary with pulse duration and shock amplitude. In Figure 8,

Table II. Acoustic and Materials Properties

Properties	Ni_3Al	Ni	Ni-60 Co
Longitudinal sound speed c_L, mm μs^{-1}	6.23 ± 0.03	5.83 ± 0.03	5.80 ± 0.03
Shear sound speed c_S, mm μs^{-1}	3.17 ± 0.03	3.03 ± 0.03	3.04 ± 0.03
Bulk sound speed c_B, mm μs^{-1}	5.04 ± 0.03	4.66 ± 0.03	4.61 ± 0.03
Ambient density ρ_0, g cm^{-3}	7.40 ± 0.01	8.90 ± 0.01	8.78 ± 0.01
Bulk modulus K, GPa	188.0	193.6	187.2
Shear modulus μ, GPa	74.4	81.7	81.1
Poisson's ratio ν	0.325	0.315	0.31
Grain size, μm	~40	~200	~100

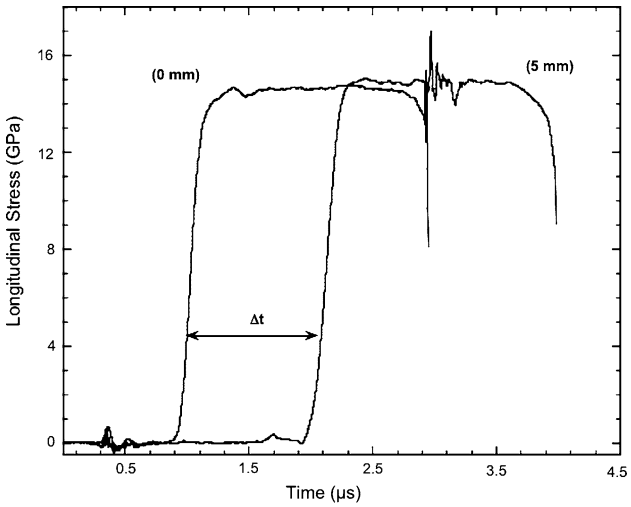

Fig. 3—Longitudinal gage traces for Ni. Stresses were induced using a 5-mm copper flyer plate at 730 m s^{-1}.

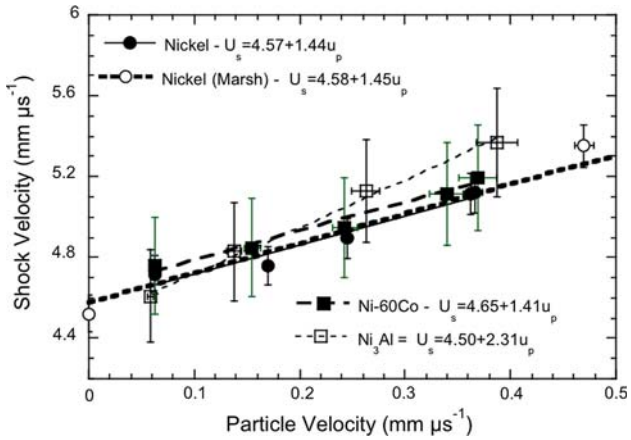

Fig. 4—Shock velocity *vs* particle velocity for Ni, Ni-60Co, and Ni_3Al.

we present the variation of spall strength with pulse duration (or in this case, specimen thickness). Simple straight lines have been fitted to indicate trends. As can be seen, each alloy displays vastly different trends. Although the trend for Ni indicates a slight decrease in spall strength, overall, we believe that there is no significant change with pulse duration. On the other hand, the Ni-60Co alloys show a clear increase, while in contrast the Ni_3Al shows a clear decrease.

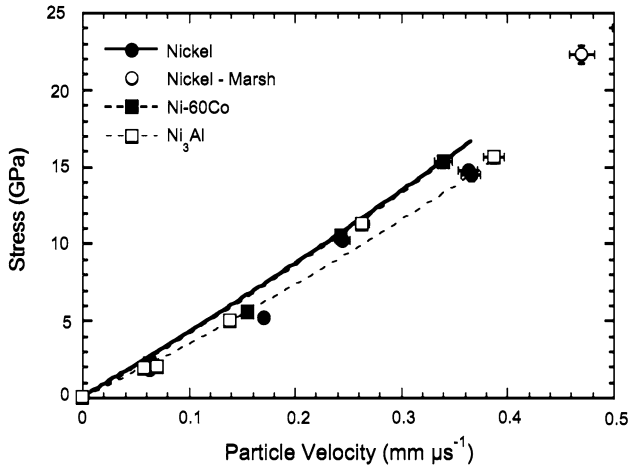

Fig. 5—Hugoniots of Ni, Ni-60Co, and Ni_3Al.

In Figure 9, the variation of spall strength with shock stress amplitude is shown. As with the effects of shock duration, clear differences can be seen in the response according to shock amplitude. Although both Ni and Ni-60Co show an increase in their spall strengths, in the case of the Ni-60Co alloy, that variation with shock stress is much greater. With Ni_3Al, the situation is somewhat more complex. Although spall strength initially increases quite rapidly (comparable to that of Ni-60Co), it reaches a peak value at ~6 GPa before decreasing at higher stresses. This significant change in spall strength is an excellent example of how alloying of the base element can lead to major differences in high-strain rate/shock-loading mechanical response.

In Figure 10, we present the variation of shear strength with shock amplitude. The values of lateral stress chosen to determine this parameter are indicated in Figure 7 by the arrows. Figure 10 demonstrates that for each alloy there is an overall increase in shear strength with increasing longitudinal stress amplitude, but as before significant differences in the responses of the three Ni-based materials is observed. It is interesting to note that the Ni-60Co displays a *lower* shear strength than the pure Ni, when one would perhaps expect as an alloyed material for it to be the stronger. In the case of the Ni_3Al, shear strength is observed to increase to a peak at an impact stress of ~6 GPa before decreasing thereafter. This is the same trend as was observed in the previous figure that plotted spall strength *vs* longitudinal

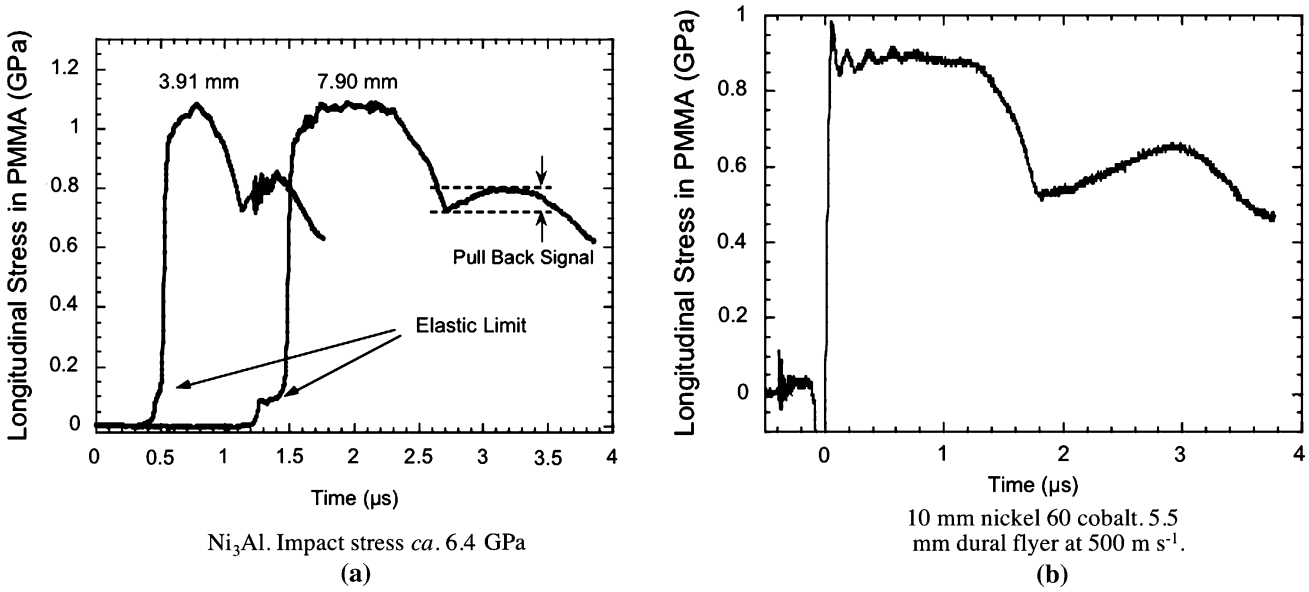

Fig. 6—Back surface gage traces in Ni alloys. (*a*) Ni_3Al, impact stress ~6.4 GPa; and (*b*) 10-mm Ni-60Co, 5.5-mm dural flyer at 500 m s^{-1}.

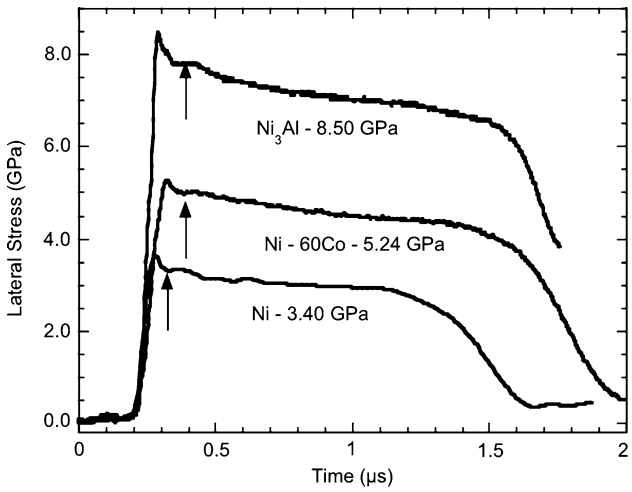

Fig. 7—Lateral stress traces in Ni, Ni-60Co, and Ni_3Al.

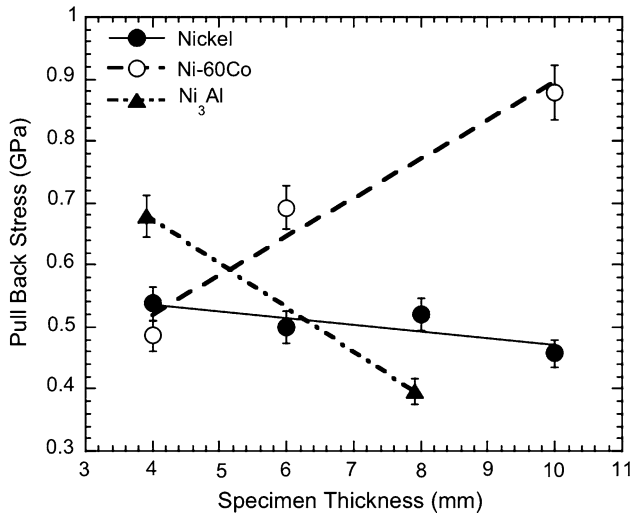

Fig. 8—Variation of spall strength with specimen thickness (pulse duration).

stress amplitude. In Figure 7, we noted that the lateral stress in all materials under investigation showed a pronounced decrease behind the shock front. In Figure 11, we quantify this change in behavior, and plot it against the longitudinal stress amplitude.

These show similar trends to what has been observed previously, with the pure Ni showing near constant behavior with amplitude, Ni-60Co increasing rapidly, and Ni_3Al reaching a peak at ~6 GPa before decreasing thereafter. Although spall (1-D tension) and shear behind the shock are reflections of very different components of strength response of materials subjected to shock wave loading, the fact that the previous four figures are each displaying similar trends for all three materials suggests common underlying mechanical and microstructural mechanisms are operating.

Finally, in Figure 12, we present optical micrographs of the recovered samples following shock loading. As detailed "soft" shock recovery sample assemblies, such as those described by Gray[17] to ensure full lateral momentum trapping were not used in these tests, contributions of an element of lateral release will have influenced the resultant microstructures in the recovered samples. Nevertheless, a qualitative assessment of the microstructural changes in the three Ni-based materials can still be made, and gross differences should be obvious.

In the case of the pure Ni, little evidence of deformation is seen to be readily observable in the recovered sample as observed using optical metallography, this being consistent with a purely dislocation based

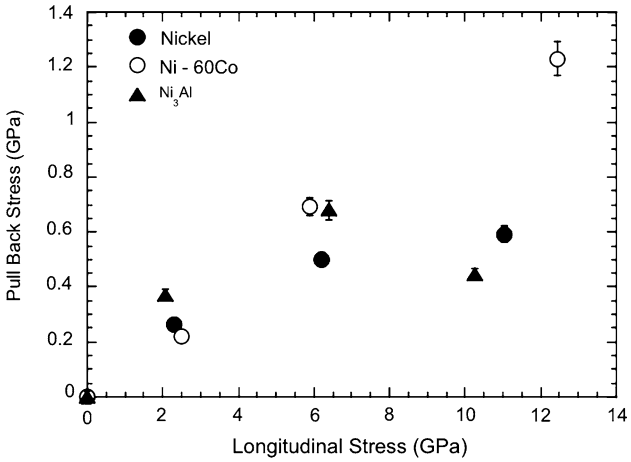

Fig. 9—Variation of spall strength with shock amplitude (at constant specimen thickness).

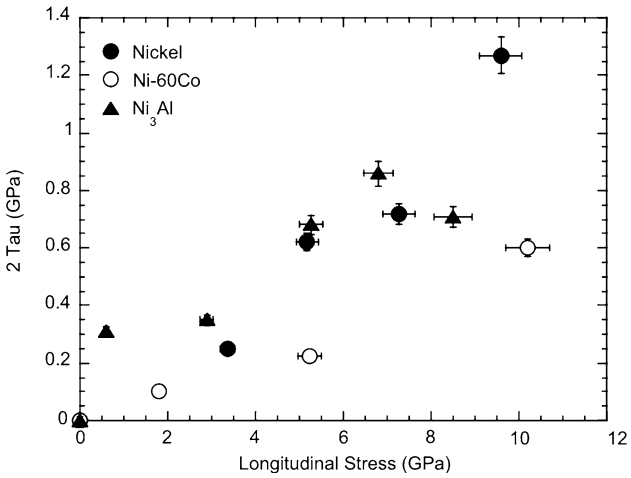

Fig. 10—Variation of shear strength with shock amplitude.

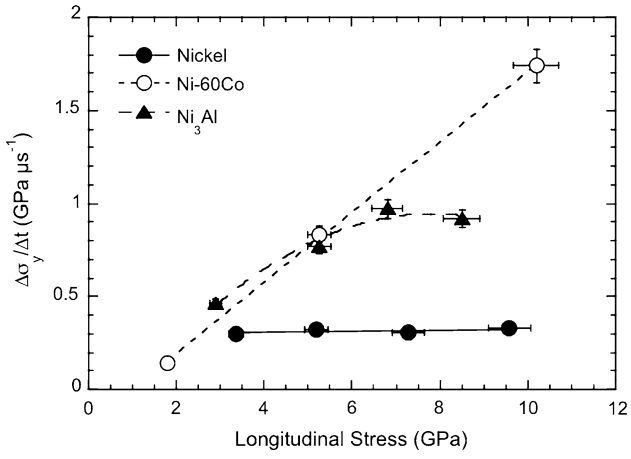

Fig. 11—Rate of change of lateral stress behind the shock front and its variation with shock amplitude.

deformation mechanism, which would not be expected to manifest itself on the optical scale. In contrast, the Ni-60Co, exhibits the presence of a significant number of deformation twins within the microstructure following shock loading. Again, this is to be expected given the low SFE of this particular alloy and the known strong dependency of twin formation on SFE. The Ni_3Al also suggests some isolated evidence of planar slip and twinning, although the sample was recovered at a lower stress. However, definitive quantification if these planar features are in fact twins requires detailed transmission electron and diffraction analysis, which is beyond the scope of the current study. The presence of twins in the Ni_3Al, if confirmed, would be consistent with the previous TEM analysis of Albert and Gray,[27] who documented deformation twinning in this material following shock prestraining.

V. DISCUSSION

The purpose of this investigation was to examine the mechanical responses of pure Ni and two Ni-based alloys subjected to shock wave loading. The two Ni-based alloys were specifically chosen to be single-phase fcc structures: Ni-60 wt pct Co possessing a reduced SFE and Ni_3Al, which represents an ordered fcc lattice-structured intermetallic. It will also be noticed that these two alloys are the basis of the two main phases present in Ni-based superalloys, namely, a solid solution based on Ni with a second intermetallic phase based on Ni_3Al. Therefore, study of these materials offers the promise of providing insight into the behavior of superalloys.

The first point to address is the shock-induced equation of state, in terms of the shock stress and shock velocity (Figures 4 and 5). From Figure 5, it can be seen that the Hugoniot (stress-particle velocity) of all three Ni-based materials displays nearly identical behavior, suggesting that the compressive responses of these materials is similar. This is a common feature previously documented within other related alloy systems, for example iron and low carbon steels[42] and tungsten-based alloys.[43] The situation with the shock velocity–particle velocity relationship (Figure 4) is somewhat more interesting. Notice that the Ni and the Ni-60Co alloy display nearly identical responses, while that of Ni_3Al is considerably steeper (a higher value of S). The values of c_0 and S derived from these curves are purely empirical. However, in simple metals, Davison and Graham[1] have suggested that c_0 (the zero particle velocity intercept of shock velocity) should correlate with the bulk sound speed, while S is related to the first pressure derivative of the bulk modulus. Concerning the latter, most materials have a value of S between 1 and 2,[35] thus making direct comparison between materials based solely on this parameter difficult. However, where the materials are related either through crystal structure or chemistry (as in the case of the three alloys under investigation in this study), a direct comparison is possible. In this case, the comparison indicates that Ni_3Al is somewhat more compressible than either pure Ni or the Ni-60Co alloy. This is

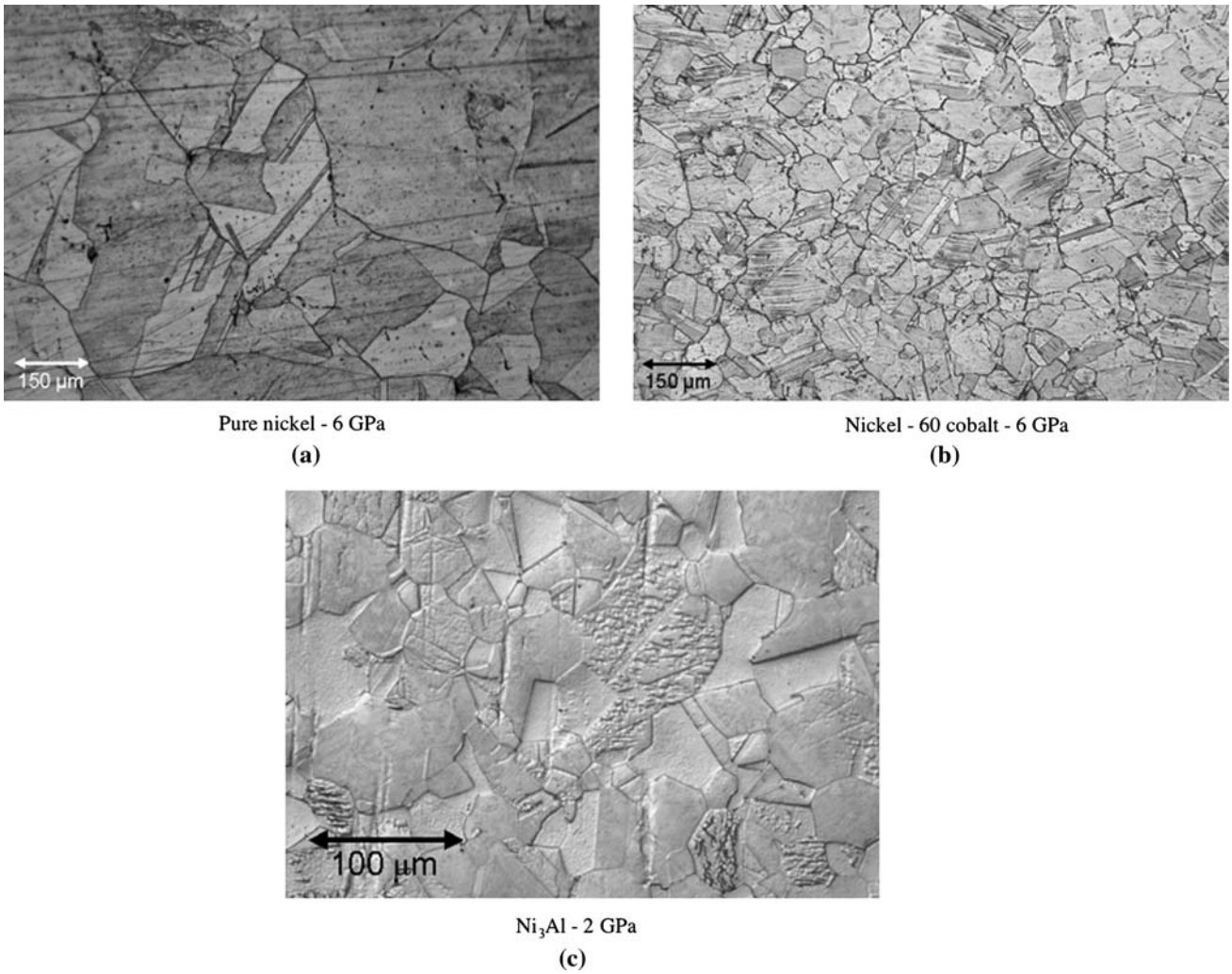

Fig. 12—Optical micrographs of recovered samples after shock loading: (*a*) pure Ni, 6 GPa; (*b*) Ni-60 Co, 6 GPa; and (*c*) Ni_3Al, 2 GPa.

somewhat surprising based on insights gleaned from the literature, given that the intermetallic has an ordered crystal structure which one might think would suggest a stiffer response to shock loading based upon the more restricted plasticity afforded through the ordered matrix structure. Examination of the three Ni-based materials data presented in Table II shows that the bulk moduli of all three Ni-based materials are nearly identical, but that the shear modulus of Ni_3Al is slightly lower and the Poisson's ratio slightly higher than the pure Ni or Ni-60Co alloy, suggesting at least a qualitative indication that the compressibility of Ni_3Al is higher than the other two Ni-based materials studied.

The major focus of this article was to quantify the effect of alloying on the mechanical response of Ni during shock loading. In doing so, we have investigated this in terms of the applied impact stress (spall strength (Figure 9) and shear strength (Figure 10)) and peak shock pulse duration (spall strength (Figure 8) and rate of change of lateral stress behind the shock front (Figure 11)). Examination of these figures suggests similarities between each measurement type (spall strength and shear strength), indicating that the underlying deformation mechanisms in Ni, Ni-60Co, and Ni_3Al control the shock-induced mechanical properties. First, the variation with shock amplitude will be considered. In terms of both spall resistance and shear strength, the same qualitative responses appear to be evident, namely, that in the case of pure Ni and the Ni-60Co, there is an increase in shear strength with peak shock amplitude, and in the case of Ni_3Al, there is an initial increase up to a peak shock stress of ~7 GPa before decreasing thereafter. However, we note with interest that in the case of spallation (Figure 9), the Ni-60Co is clearly stronger than pure Ni, while in the case of shear strength (Figure 10), the situation is reversed with Ni displaying the higher strength value. In terms of peak shock stress pulse duration, it can be seen for spallation that the pull back signal in Ni is near constant, increases for the Ni-60 wt pct Co alloy, and decreases markedly in the case of Ni_3Al. In terms of the rate of change of the lateral stress behind the shock front, the pure Ni displays a nearly constant behavior, the Ni-60Co increases its lateral stress behind the shock,

and Ni_3Al reaches a peak at ~7 GPa before decreasing again. This suggests that in the case of the latter two materials, there is a time dependence in their shock responses; *i.e.*, kinetic aspects of shock generation/storage processes are operative during shock loading in these materials.

The most straightforward results to compare between the three Ni-based materials are the shear strengths as a function of shock amplitude (Figure 10), because these measurements were taken with a manganin stress gage placed within the material during loading and thus is time independent. The most striking feature in this comparison of material responses is that the pure Ni displays a higher shear strength than the Ni-60Co, whereas it might be expected that the reverse situation would apply. An explanation can be postulated from considering the deformation mechanisms operative in each material. In the case of pure Ni, shock-induced deformation has been shown by a number of authors[15,18] to occur *via* the formation of dislocations that relax into dislocation cells. Although Ni-60Co has not been investigated specifically in terms of its shock-induced microstructure using ''soft'' shock recovery methods,[17] other low-SFE materials such as copper-aluminum alloys[4–7] have been examined in detail, and the importance of an increased incidence of deformation twinning consistent with the reduced SFE suggests itself.

In the case of Cu-Al alloys, Rohatgi *et al.*[4–7] demonstrated an increasing propensity to form deformation twins as the aluminum content increased, and thus SFE decreased. As twinning became increasingly dominant, dislocation generation and storage was less dominant. It is interesting to note that in recovered samples in the Cu-Al alloy system, postshock hardening compared to quasi-statically deformed samples was shown to decrease as the SFE decreased. On the basis of these studies it appears the efficiency of deformation twinning itself has a greatly reduced strengthening effect compared to dislocation generation and storage during shock wave loading. Comparison of the recovered microstructures in Figure 12 shows that in the Ni-60Co there is significant formation of deformation twins, while in the pure Ni shock prestrained sample, no evidence of such behavior was noted. Therefore, taking all these defect generation and storage mechanisms into consideration, it is perhaps not surprising that the pure Ni exhibits a higher shear strength than the low SFE Ni-60Co. In the case of the Ni_3Al ordered intermetallic alloy, the situation is somewhat more complex, given that the material initially strengthens, before undergoing a reduction at a shock amplitude of ~7 GPa.

The shock recovery work conducted by Albert and Gray[27] shows that Ni_3Al deforms by a mixture of dislocation activity and deformation twinning, thus one might expect a similar response to that exhibited by the Ni-60 wt pct Co alloy. However, an additional factor is clearly influencing the shock-hardening response of Ni_3Al. In the variation of spall strength with shock amplitude data for Ni_3Al (Figure 9), the same basic response with peak shock stress is repeated with a peak strength at ~7 GPa, before reducing as the peak shock stress amplitude increases. One possible cause is an increasingly brittle response, due to exhaustion in its strain hardening, as the material displays a reduced ability to accommodate the imposed strain *via* plasticity. In a previous study[34] it was noted that unlike pure Ni, which was recovered largely intact, if heavily deformed, Ni_3Al, was recovered as a series of fragments following shock prestraining, and size decreased with increasing peak shock stress amplitude. Metallographic examination of the Ni_3Al fragments displayed extensive intergranular failure with little evidence of bulk plasticity. With both pure Ni and the Ni-60Co, the alloy is clearly the stronger reversing the trends shown in Figure 10. The reasons are not immediately clear, but the differences between these two measurement techniques should be kept in mind. A shear strength measurement consists of placing a stress gage within the material subjected to shock loading, and thus can be considered time independent. In contrast, a spall measurement requires that a stress gage be supported on the rear surface of a target assembly with a block of PMMA. The spall experiment itself is designed such that the tensile interaction between releases from the rear of the flyer plate and target take place within the target plate. Therefore, the stress gage is remote from this location and is dependent upon information being transmitted from the spall plane to the rear surface. Further, this type of measurement is also time integrated as the sample will have been loaded to a peak shock stress, held at that peak shock stress defined by the thickness of the flyer plate, and partially unloaded before spallation is induced within the sample material. The combined effect of all of these factors is known to be complex and thus, will have a significant effect upon the final response of the material subjected to spallation loading.

The pulse duration effects are equally illuminating. In Figure 8, the variation of spall strength with specimen thickness (in effect duration) shows that for the pure Ni the spall strength is near constant, the Ni-60Co displays a rapid increase, and Ni_3Al shows a decrease. From a discussion of the previous results and their variations with peak shock stress amplitude, combined with the observations of others[27] showing that Ni_3Al accommodates some of the shock-induced plasticity by twinning, might lead one to expect it to behave in a similar manner to the Ni-60Co. However, the intergranular failure demonstrated in a previous work[34] suggests that brittle fracture also has an important role in the shock-induced deformation of Ni_3Al. A reduction in spall strength with pulse duration has also been observed in various grades of alumina.[51] Although this issue was not specifically addressed in the previous work in the literature, it would seem likely that brittle failure would have a significant role, and thus we believe that at least some of the spall response of Ni_3Al is controlled in a similar fashion. In the case of pure Ni, the fact that the spall strength appears to be nearly constant as a function of pulse duration suggests that the shock-induced microstructure reaches its equilibrium state quite quickly. In contrast, the Ni-60Co deformation takes longer to reach this equilibrium, and the results presented here suggest that for the imposed loading conditions has not reached that point. A similar

situation is presented in Figure 11, where the rate of change of the lateral stress with time (behind the shock front) with peak shock stress amplitude shows that the behavior of pure Ni is nearly constant, the Ni-60Co rapidly increases, and Ni_3Al reaches a peak response at ~7 GPa peak shock stress before leveling or decreasing slightly.

Taking all of these results into account, it is possible to propose how these variations of alloying affect the response of Ni and its alloys to shock loading. In the case of pure Ni, the response is well known with Murr and Kuhlmann-Wilsdorf[12] showing that it deforms *via* dislocation generation and storage in well-formed cells, reaching steady state conditions (at ~20 GPa) between 0.5 and 1 μs. As SFE is reduced (as in the case in the Ni-60Co or Cu-Al alloys discussed earlier), the separation of partial dislocations increases, thus reducing the effective mobility of dislocations to cross-slip and therefore work-harden *via* the storage of increasing dislocation line length. Under shock loading conditions, the mobility of these partials will be low enough that not all of the applied deformation can be accommodated by dislocation generation and motion, hence deformation twinning becomes increasingly important. However, the results (and in particular the variation of the spall strength with pulse duration at peak shock stress), suggests that twin formation occurs extremely rapidly, possibly within the shock front itself, and that further deformation is accommodated *via* dislocation generation and storage. In contrast, Ni (which deforms principally *via* dislocation generation) reaches a steady state quite quickly, hence the stable behavior shown in Figures 8 and 11. However, these results also suggest that if measurements were made in pure Ni at very short pulse durations, a hardening response might well be observed consistent with the results of Follansbee and Gray.[16]

The brittle behavior of shock-loaded Ni_3Al is somewhat surprising, given that the aluminum lean, boron-doped composition studied in this work would suggest that it should be ductile based on literature data. In fact, its response is reminiscent of ''pure'' Ni_3Al deformed at quasi-static strain rates. The role of boron has been discussed by a number of authors,[21,23,52] where it has been suggested that it segregates to grain boundaries thereby strengthening them, or to dislocations and superlattice intrinsic stacking faults (SSIFs). In the case of the latter, it has been proposed that boron modifies SSIF dissociated superdislocation to antiphase boundary (APB) bounded pairs, thus increasing their mobility. This would have the effect of ''softening'' the grain interiors, and thus reducing the discrepancy in strength between the grains and their boundaries, thus facilitating transmission of slip across grain boundaries. Therefore, two possible mechanisms exist to explain the low ductility in the shock-loaded Ni_3Al. First, the extreme strain rates encountered during shock loading would, through the generation of Kear–Wilsdorf locks,[24] result in very high rates of work hardening within the grains, thus increasing the strengths of those grains relative to the grain boundaries and increasing the likelihood of grain boundary failure. Alternatively, we need to consider the role of boron itself. At quasi-static strain rates deformation is dependent in part at least on the modification of dislocations. Due to the interstitial nature of boron's solution in Ni_3Al its diffusion velocity will be high, and thus under quasi-static strain rates it will be able to move with the dislocations themselves. However, during shock loading dislocation motion will be extremely fast, and the boron will be unable to move with the dislocations. As some of the boron will have segregated to those dislocations, they will be moving into boron-deficient regions. In effect, the Ni_3Al will be behaving as though no boron is present. Therefore, it appears as though the ductilization of Ni_3Al with boron is less effective at shock-induced strain rates.

VI. CONCLUSIONS

A series of plate impact experiments have been performed on pure Ni, Ni-60Co, and Ni_3Al to investigate the effects of solid solution alloys and crystallographic ordering on the shock response of Ni-based alloys. In the case of the solid solution alloy, Ni-60Co, the reduction in the SFE led to a shift from a purely dislocation-based deformation mechanism to one more dominated by deformation twin formation. This was manifest in the shock-induced mechanical properties as a decrease in shear strength behind the shock front, an increase in the hardening rate behind the shock front, and a strong positive dependence upon pulse duration of the dynamic tensile (spall) strength. It has been proposed that the shift from dislocation to twin dominated deformation has increased the time taken for the deformation microstructure to reach its steady state, and thus manifests itself on the measured post-shock prestrained mechanical properties. In the case of Ni_3Al, it has been shown that the material, while undergoing an initial increase in spall and shear strength with increasing peak shock amplitude, shows a subsequent decrease a stresses greater than ~7 GPa. It has also been shown that spall strength reduces with pulse duration as well. In combination with recovery experiments from a previous work, we believe that some of the applied shock-induced deformation is accommodated by brittle failure, in contrast to the expected ductility displayed at quasi-static strain rates. We believe that under shock loading conditions, dislocation motion is so fast that boron is effectively removed from the mobile dislocations, thus rendering boron-assisted ductility ineffective.

ACKNOWLEDGMENTS

The authors thank Dr. Yann Meziere, Ivan Knapp, Matt Eatwell, and Adrian Mustey, Cranfield University, and Dr. Ellen Cerreta, Los Alamos National Laboratory, for their assistance in this program. This research was funded by the Engineering and Physical Sciences Research Council (Grant No. GR/S07476/01).

REFERENCES

1. L.W. Davison and R.A. Graham: *Phys. Rep.*, 1979, vol. 55, pp. 255–379.
2. M. Hansen: *Constitution of Binary Alloys*, McGraw-Hill, London, 1958, pp. 485–87.
3. P.C.J. Gallagher: *Metall. Trans.*, 1970, vol. 1, pp. 2429–61.
4. A. Rohatgi and K.S. Vecchio: *Mater. Sci. Eng.*, 2002, vol. A328, pp. 256–66.
5. A. Rohatgi, K.S. Vecchio, and G.T. Gray III: *Metall. Mater. Trans. A*, 2001, vol. 32A, pp. 135–45.
6. A. Rohatgi, K.S. Vecchio, and G.T. Gray III: *Acta Mater.*, 2001, vol. 49, pp. 427–38.
7. A. Rohatgi, K.S. Vecchio, and G.T. Gray III: in *Fundamental Issue and Applications of the Shock-Wave and High-Rate Phenomena*, K. Staudhammer, L. Murr and M. Meyers, eds., Elsevier, Amsterdam, 2001, pp. 25–32.
8. R.F. Trunin, M.Y. Belakiova, M.V. Zhernokletov, and Y.N. Sutulov: *Izv. Akad. Nauk. SSSR, Fiz Zemli (Bull. Acad. Sci. USSR, Phys. Solid Earth)*, 1991, pp. 99–109.
9. M.F. Rose, T.L. Berger, and M.C. Inman: *Trans. TMS-AIME*, 1967, vol. 239, pp. 1998–99.
10. H. Kressel and N. Brown: *J. Appl. Phys.*, 1967, vol. 38, pp. 1618–25.
11. F.I. Grace: *J. Appl. Phys.*, 1969, vol. 40, pp. 2649–53.
12. L.E. Murr and D. Kuhlmann-Wilsdorf: *Acta Metall.*, 1978, vol. 26, pp. 847–57.
13. R.N. Wright and D.E. Mikkola: *Mater. Sci. Eng.*, 1982, vol. 53, pp. 273–83.
14. F. Greulich and L.E. Murr: *Mater. Sci. Eng.*, 1979, vol. 39, pp. 81–93.
15. M.A. Meyers, H.J. Kestenbach, and C.A.O. Soares: *Mater. Sci. Eng.*, 1980, vol. 45, pp. 143–52.
16. P.S. Follensbee and G.T. Gray III: *Int. J. Plast.*, 1991, vol. 7, pp. 651–60.
17. G.T. Gray III: in *Shock-Wave and High Strain Rate Phenomena in Materials*, M.A. Meyers, L.E. Murr and K.P. Standhammer, eds., Marcel Deker, New York, NY, 1992, pp. 899–911.
18. L.E. Murr and J.-Y. Huang: *Mater. Sci. Eng.*, 1975, vol. 19, pp. 115–22.
19. D.P. Dandekar and A.G. Martin: in *Shock Waves and High-Strain-Rate Phenomena in Metals*, M.A. Meyers and L.E. Murr, eds., Plenum, New York, NY, 1980, pp. 573–87.
20. E.B. Zaretsky, G.I. Kanel, S.V. Razorenov, and K. Baumung: *Int. J. Imp. Eng.*, 2005, vol. 31, pp. 41–54.
21. K. Aoki: *Mater. Trans. JIM*, 1990, vol. 31, pp. 443–48.
22. I. Baker, D.V. Viens, and E.M. Schulson: *Scripta Metall.*, 1984, vol. 18, pp. 237–40.
23. N. Mashahashi, T. Takasugi, and O. Izumi: *Acta Metall. Mater.*, 1988, vol. 36, pp. 1823–36.
24. B.H. Kear and H.G.F. Wilsdorf: *Trans. TMS-AIME*, 1962, vol. 224, pp. 382–86.
25. H.W. Sizek and G.T. Gray III: *Acta Metall. Mater.*, 1993, vol. 41, pp. 1855–60.
26. G.T. Gray III: in *High Pressure Science and Technology*, S.C. Schmidt, G.A. Samara and M. Ross, eds., AIP Press, Colorado Springs, CO, 1993, pp. 1161–64.
27. D.E. Albert and G.T. Gray III: *Phil. Mag. A*, 1994, vol. 70, pp. 145–58.
28. N.V. Kasantseva, B.A. Greenberg, A.A. Popov, and E.V. Shorokhov: *J. Phys. IV*, 2003, vol. 110, pp. 923–28.
29. H.Y. Geng, N.X. Chen, and M.H.F. Sluiter: *Phys. Rev. B*, 2005, vol. 71, p. 012105.
30. I. Song and N.N. Thadhani: in *Shock Compression of Condensed Matter-1989*, S.C. Schmidt, J.N. Johnson and L.W. Davison, eds., North-Holland, Albuquerque, NM, 1990, pp. 499–502.
31. N.N. Thadhani: in *Shock Compression of Condensed Matter-1989*, S.C. Schmidt, J.N. Johnson and L.W. Davison, eds., North-Holland, Albuquerque, NM, 1990, pp. 503–10.
32. Y. Meziere, J.C.F. Millett, and N.K. Bourne: *Int. J. Imp. Eng.*, 2007, vol. 34, pp. 360–76.
33. J.C.F. Millett, Y.J.E. Meziere, and N.K. Bourne: *J. Mater. Sci.*, 2007, vol. 42, pp. 5941–48.
34. J.C.F. Millett, Y.J.E. Meziere, G.T. Gray III, E.K. Cerreta, and N.K. Bourne: *J. Appl. Phys.*, 2006, vol. 100, p. 063506.
35. S.P. Marsh: *LASL Shock Hugoniot Data*, University of California Press, Los Angeles, CA, 1980.
36. N.K. Bourne: *Meas. Sci. Technol.*, 2003, vol. 14, pp. 273–78.
37. Z. Rosenberg, D. Yaziv, and Y. Partom: *J. Appl. Phys.*, 1980, vol. 51, pp. 3702–05.
38. Z. Rosenberg and Y.J. Partom: *J. Appl. Phys.*, 1985, vol. 58, pp. 3072–76.
39. J.C.F. Millett, N.K. Bourne, and Z. Rosenberg: *J. Phys. D.*, 1996, vol. 29, pp. 2466–72.
40. Z. Rosenberg, N.K. Bourne, and J.C.F. Millett: *Meas. Sci. Technol.*, 2007, vol. 18, pp. 1843–47.
41. G.T. Gray III: in *High-Pressure Shock Compression of Solids*, J.R. Asay and M. Shahinpoor, eds., Springer-Verlag, New York, NY, 1991, pp. 187–215.
42. N. Bourne and J. Millett: *Scripta Mater.*, 2000, vol. 43, pp. 541–46.
43. J.C.F. Millett, N.K. Bourne, Z. Rosenberg, and J.E. Field: *J. Appl. Phys.*, 1999, vol. 86, pp. 6707–09.
44. N.K. Bourne and Z. Rosenberg: *Meas. Sci. Technol.*, 1997, vol. 8, pp. 570–73.
45. J.C.F. Millett, N.K. Bourne, G.T. Gray III, and I.P. Jones: *Acta Mater.*, 2002, vol. 50, pp. 4801–11.
46. Y.J.E. Meziere, J.C.F. Millett, and N.K. Bourne: *J. Appl. Phys.*, 2006, vol. 100, p. 033513.
47. A. Hopkins and N.S. Brar: in *Shock Compression of Condensed Matter-1999*, M.D. Furnish, L.C. Chhabildas and R.S. Hixson, eds., American Institute of Physics, Melville, New York, NY, 2000, pp. 423–26.
48. J.C.F. Millett and N.K. Bourne: *J. Appl. Phys.*, 2000, vol. 88, pp. 7037–40.
49. J.C.F. Millett, N.K. Bourne, and N.R. Barnes: *J. Appl. Phys.*, 2002, vol. 92, pp. 6590–94.
50. J.C.F. Millett, G.T. Gray III, and N.K. Bourne: in *Shock Compression of Condensed Matter-2003*, M.D. Furnish, Y.M. Gupta and J.W. Forbes, eds., AIP Press, Melville, NY, 2004 , pp. 663–66.
51. N.H. Murray, N.K. Bourne, Z. Rosenberg, and J.E. Field: *J. Appl. Phys.*, 1998, vol. 84, pp. 734–38.
52. J.A. Horton and M.K. Miller: *Mater. Res. Symp. Proc.*, 1987, vol. 81, pp. 105–10.